

Study on Strength Characteristics and Constitutive Model of Frozen Sulfate Saline Silty Clay under High Confining Pressure

Zhiyi Liu¹⁾, Yu Song²⁾, Fengxi Zhou^{3)*} and Liye Wang⁴⁾

¹⁾ School of Civil Engineering, Lanzhou University of Technology, Lanzhou, 730050, China;
School of Civil Engineering, HeXi University of Technology, Zhangye, 734000, China.

²⁾ School of Civil Engineering, Lanzhou University of Technology, Lanzhou, 730050, China.

³⁾ School of Civil Engineering, Lanzhou University of Technology, Lanzhou, 730050, China.

* Correspondent Author. E-Mail: geolut@163.com.

⁴⁾ School of Civil Engineering, Lanzhou University of Technology, Lanzhou, 730050, China.

ABSTRACT

To explore the deformation behavior and failure strength of sulfate saline silty clay at a temperature of -10°C and confining pressures of 6~10 MPa, we have performed low-temperature triaxial shear tests on sulfate saline silty clay in Hexi region of Gansu province, China. The variation trend of deviatoric stress, volumetric strain and initial deformation modulus with confining pressure were analyzed. The results demonstrated that the stress-strain curve of frozen sulfate saline silty clay was hyperbolic and the deviatoric stress increased as the axial strain increased and was eventually constant. Owing to particle breakage and melting of ice, when the confining pressure $\sigma_3 > 6$ MPa, the strength decreased as the confining pressure increased and the sample exhibited volumetric shrinkage throughout the entire confining-pressure range. A constitutive model of frozen sulfate saline silty clay under high confining pressure has been proposed in combination with the Duncan-Chang model and the validity of the model has been confirmed by comparison with test data.

KEYWORDS: Frozen sulfate saline soils, Strain hardening, Volumetric contraction, Strength criterion, Triaxial-compression tests.

INTRODUCTION

Saline soil is widely distributed in China, especially in the cold climates of the northwest, north and northeast regions, accounting for approximately 69.03% of the distribution region of saline soil in China (Yang, 2008). The presence of salt makes the physico-mechanical qualities of frozen saline soil in cold climates more complex than those of ordinary frozen soil (Xu et al., 2016; Zhao et al., 2020a).

Frozen saline soil is composed of gas, ice, soil particles, unfrozen water, salt crystals and other components (Chang et al., 2019). Minor changes in temperature, water content, confining pressure, salt content and other external factors greatly influence the composition of saline soil, resulting in dramatic changes in its physico-mechanical properties. In the past few

decades, scholars have conducted a series of triaxial or uniaxial compression tests on saline soil under negative temperature in terms of water content (Xu et al., 2019; Cai et al., 2014), salt content (Zhao et al., 2020a; Liao et al., 2016), confining pressure (Liao et al., 2016; Xu et al., 2016; Xu et al., 2017), temperature (Xu et al., 2016; Zhao et al., 2020b; Zhang et al., 2017), strain rate (Gao et al., 2019) and number of freeze-thaw cycles (Han et al., 2018; Xu et al., 2019; Zhang et al., 2019), discussing the mechanical-deformation behavior of frozen saline soil and proposing several constitutive models to depict the mechanical properties of frozen saline soil. Zhao et al. (2020a, 2020b) developed a dynamic-strength criterion and an anisotropic-boundary surface elastic-plastic constitutive model of frozen sulfate saline soil under cyclic loading. Liao et al. (2016) introduced a weighting factor into the Matsuoka-Nakai and Lade-Duncan strength criterion. Zhang et al. (2019) discussed the impact of the confining pressure, consolidation method and stress path on the strength of frozen saline

Received on 16/3/2023.

Accepted for Publication on 18/8/2023.

silty soil. Yang et al. (2008) used the Duncan-Chang hyperbolic model to obtain the initial elastic modulus and maximum deviatoric stress of frozen saline soils, as well as the change of initial elastic modulus and deviatoric stress with salt content and temperature. Gao and Lai (2018) used the generalized nonlinear theory to determine the strength criterion of frozen saline soil, considering the influence of loading rate. Furthermore, they analyzed the influence of loading rate on strength and internal friction angle. Lai et al. (2007) developed a modified Duncan-Chang model that can depict both strain hardening and softening for the stress-strain curve of frozen sand and its accuracy was better than that of the Mohr-Coulomb strength criterion. Hu and Lai (2014) proposed a nonlinear strength criterion for frozen saline silty sand, that could accurately describe the change rule of shear strength with the confining pressure. Luo et al. (2019) developed a strength criterion for frozen saline soil based on a binary-medium model. Liu et al. (2019) discussed the types of frozen-soil strength curves and provided formulae for calculating the internal friction angle and cohesion. Niu et al. (2022) provided a strength criterion for frozen silty clay that considered water content.

So far, scholars have achieved detailed results in research on the strength of sulfate saline soil under negative temperatures. Constitutive models have been proposed to depict the mechanical characteristics of frozen sulfate saline soil. However, there are few reports on the strength-deformation of frozen sulfate saline soils under high confining pressures. Through an on-the-spot investigation of the Zhang Ye region of the Lan Xin high-speed railway, it was found that the sub-grade in this region has evident bulges, cracks, shedding and other engineering defects at different depths, where the defects worsen with increasing depth. Consulting local data, it was preliminarily determined that the soil in this region is typical sulfate saline soil, the groundwater level is about 2.0 m deep, the lowest temperature in winter is -15°C , the highest temperature in summer is 37°C and the altitude is 1500 m, which is typical of arid climate. In this study, the sulfate saline silty clay near the Lan Xin high-speed railway in Zhangye city, Gansu province, China, is selected as the research object. After salt washing, the soil sample with a salt content of 1.5% and a water content of 15% was remolded. Triaxial-shear tests were carried out

at a temperature of -10°C and confining pressures of 6~10 MPa. We have discussed the strength and deformation behavior of frozen sulfate saline silty clay under high confining pressure and the strength criterion of frozen sulfate saline silty clay under high confining pressure. It is expected to provide a reference for engineering construction and aid engineering-defect prevention in similar saline soil regions.

METHODOLOGY

Material and Specimen Preparation

To clarify the physico-mechanical behavior of frozen sulfate saline silty clay under high confining pressure, low-temperature triaxial-shear tests were conducted on sulfate saline silty clay. The test soil was obtained from a site near the Lan Xin high-speed railway in WuJiang Town, Gan Zhou district, Zhang Ye city, Gansu province, China, as shown in Fig. 1.

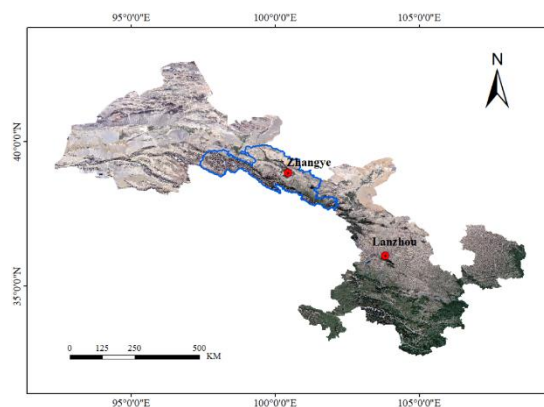


Figure (1): The location of sampling

The natural burial depth of the soil was approximately 1.2 m and the initial water content was 13.2%. Through the analysis of soluble salts, it was found that the undisturbed soil was a typical sulfate saline soil with a salt content of 1.01%. To eliminate the impact of other ions on mechanical deformation, the soil samples were desalinated. Simultaneously, the change of salt in soil was monitored with a salinometer. Desalting was considered complete when the total salt content was $< 0.1\%$. After desalting, the soil sample was prepared by drying, crushing and sieving (2 mm). Additionally, the basic physical indices of the soil in the Hexi region of Gansu province, after desalting and drying, were obtained, as shown in Table 1, where the soil was determined to be a silty clay soil.

Table 1. Basic physical parameters of natural saline soil

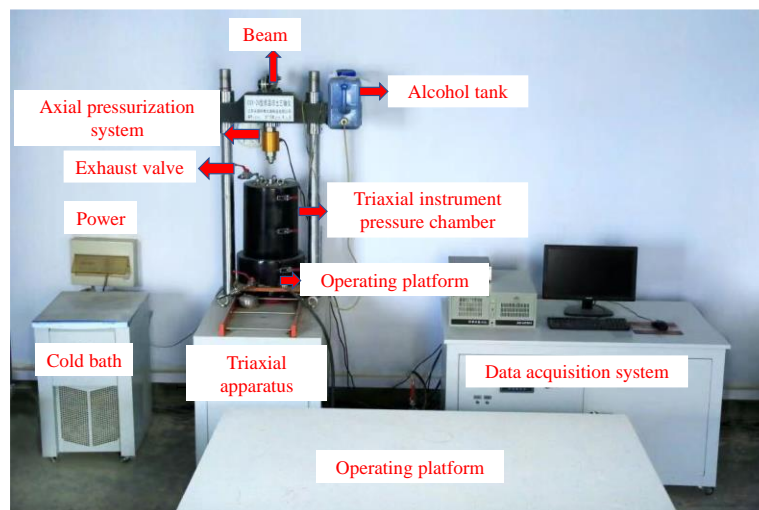
Particle size composition %			Liquid limit	Plastic limit	Maximum dry density	Optimum water content
>0.005mm	0.075~0.005mm	<0.005mm				
18.1	64.2	17.7	29.2%	13.5%	1.88 g·cm ⁻³	15%

To study the impact of high confining pressure on the strength and deformation characteristics of frozen sulfate saline silty clay, the salt content of the remodeled sample was controlled at 1.5%, while the water content was controlled at 15%. The sample-preparation steps were as follows: Firstly, the desalted and dried silty clay was mixed with 1.5% sodium sulfates and fully stirred to evenly distribute the salt in the soil. Secondly, distilled water with a target water content of 15% was added and the mixture was stirred evenly. Considering the uniformity of water and salt, distribution, the soil sample was mixed evenly in the fresh-keeping bag, sealed and placed in a storage box for 24 h. Then, a certain mass of soil was taken, subjected to split loading and layered compaction (seven layers in total) and made into a cylindrical specimen with a diameter of 100 mm and a height of 200 mm. Vaseline was applied to the inner wall of the sample preparation barrel to reduce friction between the soil and the cylinder wall for easy

mold removal. Finally, the prepared sample was kept together with the mold in a refrigeration box at -30°C for quick freezing, avoiding the formation of a visible ice interlayer during the freezing process. After 48 h, an epoxy-resin gasket was placed on both ends of the sample and the sample was put into the rubber film and placed in a constant-temperature box at the same test temperature for 24 h.

Test Methods

The test was conducted using CSY-20 low-temperature frozen soil triaxial equipment, as shown in Fig. 2. The CSY-20 low-temperature frozen soil triaxial equipment comprises a pressure-testing machine, a triaxial-pressure chamber, a pressure console, a cold bath and a data-acquisition system. The accuracy of temperature regulation is $\pm 0.1^\circ\text{C}$. Axial loading was managed by strain control, at a loading rate of 1 mm/min.

**Figure (2): CSY-20 low-temperature frozen soil triaxial apparatus**

The test steps were as follows:

- (1) Filling: the sample cured in the thermostat for 24 h was quickly removed and placed into the triaxial-pressure chamber and then, temperature-controlled alcohol at the same temperature as the test

temperature was injected into the pressure chamber.

- (2) Fixing: the motor was started, the axial pressure piston was controlled to make full contact with the top of the sample and the displacement sensor was installed and fixed.

- (3) Pressurizing: a pre-set confining pressure was applied. After the confining pressure stabilized, a constant confining pressure was maintained for 30 min.
- (4) Shearing: the displacement sensor, body-pressure sensor and pore-pressure sensor were adjusted to make their readings return to zero. Then, an axial load was applied at an axial-deformation rate of 1mm/min until the sample was sheared and damaged.

The data-acquisition system collected data once every 10 s. The test was terminated when the axial deformation reached 30 mm. The confining pressure was removed and the sample was also removed. The whole test lasts about 45 min. After the test, the corresponding stress-strain-volume changes were calculated according to the collected data and the test results were analyzed.

RESULTS AND ANALYSIS

Triaxial-shear Test Results

The frozen sulfate saline silty clay sample underwent plastic deformation after triaxial shearing and its shape was compressed from the initial cylinder to a middle bulge. Fig. 3 illustrates the failure modes. Fig. 4(a) shows the relationship curve of the deviatoric stress-axial strain of the frozen sulfate saline silty clay under different confining pressures. As shown in Fig. 4(a), $(\sigma_1 - \sigma_3) - \varepsilon_a$, (σ_1, σ_3) and $(\sigma_1 - \sigma_3)$ were axial stress, confining pressure and deviatoric stress, while ε_a was axial strain. Curves of the frozen sulfate saline silty clay samples were very similar in all confining-pressure ranges and were mostly hyperbolic. Based on research on the stress-strain curve of frozen soil (Ma and Chang, 2002; He et al., 2022) and the results of this experiment,

the stress-strain curve can be broadly divided into three stages. The first stage (oc segment) is also known as the elastic stage, where the stress linearly increases with the strain increase, primarily owing to the strength and deformation of ice. The second stage (cd segment) is the elasto-plastic stage which mainly corresponds to the strength and deformation of the soil and the deformation is mostly plastic including a part of elastic deformation. The third stage (after point d) is the failure stage. Additionally, the axial deviatoric stress first increased rapidly as the strain increased and then increased slowly and tended to be constant. The curve exhibited no obvious peaks and the hardening phenomenon was evident. For a curve without a peak point, the deviatoric stress corresponding to $\varepsilon_a = 15\%$ was considered as the failure strength of the sample. As shown in Fig. 4(a), the confining pressure has a considerable impact on the strength of frozen sulfate saline silty clay, particularly when $\sigma_3 > 6\text{MPa}$, where the strength decreases as the confining pressure increases owing to ice melting and crushing, which is consistent with the results of Niu et al. (2019) and Ma and Chang (2002).

Fig. 4(b) exhibits the volume strain-axial strain relationship curves of the frozen sulfate saline silty clay. The sample exhibited a volumetric shrinkage throughout the entire confining-pressure range and the volumetric shrinkage gradually decreased with an increase in the confining pressure, ultimately reaching a constant value. The reason for this is that before applying shear stress to the sample, the sample was already consolidated under constant confining pressure for 30 min. and the volume had shrunk. Furthermore, the greater the confining pressure, the greater the degree of compaction. However, the greater the confining pressure, the greater the ability to limit shear deformation when applying shear stress.



Figure (3): Failure modes of frozen sulfate saline silty clay samples after triaxial-shear tests

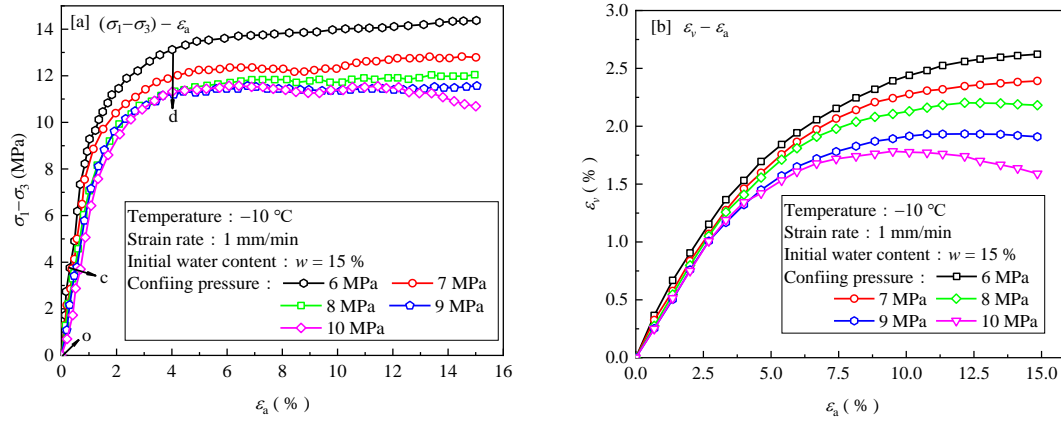


Figure (4): The stress-strain curves of frozen sulfate saline silty clay under various pressures

Strength Criterion of Frozen Sulfate Saline Silty Clay

The failure loads of geotechnical materials were evaluated using the strength criterion. Several scholars have proposed numerous strength criteria for unfrozen soil, such as the von Mises-Botkin criterion, the Drucker-Prager criterion and the Mohr-Coulomb criterion.

Studies have shown that the Mohr-Coulomb strength criterion can still be used to predict the strength of soil under low confining pressures; however, it is no longer effective under high confining pressures. For this reason, strength criteria for frozen soil under various confining pressures have been proposed (Chang et al.,

2019; Zhang et al., 2017; Fu et al., 2020) and the strength-deformation characteristics of frozen soil under various confining pressures have been analyzed in detail. Owing to the particularity of the structure of frozen saline soil and the complexity of its composition, the strength criteria proposed in the past are still applicable to frozen saline soil. Therefore, this study conducted low-temperature triaxial-shear tests and analyzed the strength characteristics of frozen sulfate saline soil under high confining pressures.

According to the results of the triaxial-shear test, the relationship curve between the maximum deviatoric stress $(\sigma_1 - \sigma_3)_{max}$ and the confining pressure σ_3 when the soil sample is damaged, is depicted in Fig. 5.

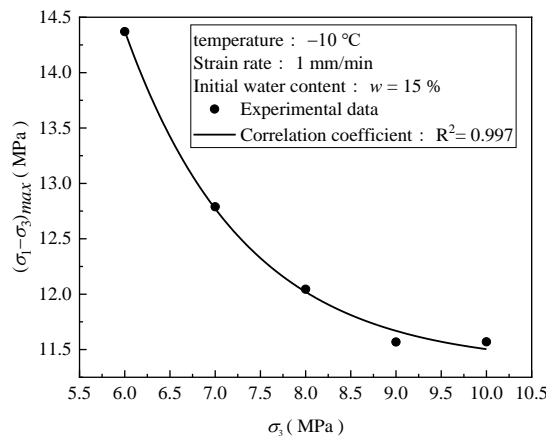


Figure (5): The relationship between the maximum deviatoric stress $(\sigma_1 - \sigma_3)_{max}$ and the confining pressure σ_3

The following functional relationship was obtained through fitting:

$$(\sigma_1 - \sigma_3)_{max} = \sigma_0 + m e^{-(\sigma_3/n)} \tag{1}$$

where: $(\sigma_1 - \sigma_3)_{max}$ represents the maximum axial deviatoric stress, while σ_0 , m and n are material coefficients. In this experiment, $\sigma_0 = 11.36$, $m=285.26$,

$n=1.32$ and $R^2=0.997$.

When the confining pressure $\sigma_3 > 6\text{MPa}$, owing to the pressure melting of ice under high confining pressure and the cracking and sliding of ice inside the frozen soil, the maximum deviator stress decreased with an increased confining pressure, finally tending to a constant value.

On the $\sigma - \tau$ stress plane, the expressions of the Mohr stress circle denoted by σ_1 and σ_3 are as follows (Liu et al., 2019):

$$f(\tau, \sigma, \sigma_1, \sigma_3) = \tau^2 - \left(\frac{\sigma_1 - \sigma_3}{2}\right)^2 + \left(\sigma - \frac{\sigma_1 + \sigma_3}{2}\right)^2 = 0 \quad (2)$$

Rewriting Eq. (1) yields:

$$g(\sigma_1, \sigma_3) = \sigma_0 + \sigma_3 - \sigma_1 + me^{-(\sigma_3/n)} = 0. \quad (3)$$

As σ_1 and σ_3 are independent of each other, the partial derivatives of Eqs. (2) and (3) can be obtained as:

$$\frac{\partial f(\sigma, \tau, \sigma_1, \sigma_3)}{\partial \sigma_1} = \sigma_3 - \sigma \quad (4)$$

$$\frac{\partial f(\sigma, \tau, \sigma_1, \sigma_3)}{\partial \sigma_3} = \sigma_1 - \sigma \quad (5)$$

$$\frac{\partial g(\sigma_1, \sigma_3)}{\partial \sigma_1} = -1 \quad (6)$$

$$\frac{\partial g(\sigma_1, \sigma_3)}{\partial \sigma_3} = 1 - \frac{m}{n} e^{-(\sigma_3/n)} \quad (7)$$

According to the envelope theory (Lai et al., 2009):

$$\frac{\partial f}{\partial \sigma_1} \frac{\partial g}{\partial \sigma_3} - \frac{\partial f}{\partial \sigma_3} \frac{\partial g}{\partial \sigma_1} = (\sigma_3 - \sigma) \left(1 - \frac{m}{n} e^{-(\sigma_3/n)}\right) + (\sigma_1 - \sigma) = 0 \quad (8)$$

From Eq. (8):

$$\sigma = \frac{\sigma_1 + \left[1 - (m/n)e^{-(\sigma_3/n)}\right] \sigma_3}{2 - (m/n)e^{-(\sigma_3/n)}} \quad (9)$$

Substituting Eq. (9) into Eq. (2) yields:

$$\tau^2 = \left(\frac{\sigma_1 - \sigma_3}{2}\right)^2 - \left\{ \frac{\sigma_1 + \left[1 - (m/n)e^{-(\sigma_3/n)}\right] \sigma_3}{2 - (m/n)e^{-(\sigma_3/n)}} - \frac{\sigma_1 + \sigma_3}{2} \right\}^2 \quad (10)$$

Eqs. (1), (9) and (10) are nonlinear expressions for the strength criterion for frozen sulfate saline silty clay. As shown in Fig. 6, when the Mohr circles are tangential

to the shear-strength envelope, the saline-soil sample is damaged and loses its ability to resist shear failure.

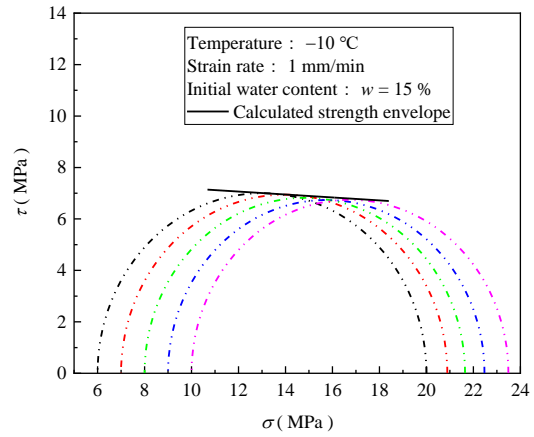


Figure (6): The shear-strength envelope curve of frozen sulfate saline silty clay

Constitutive Model of Frozen Saline Soil

As illustrated in Fig. 4(a), most of the stress-strain curves of the frozen sulfate saline silty clay are hyperbolic and show a strain-hardening phenomenon, which can be generally described by the Duncan - Chang model (Sun et al., 2014):

$$\sigma_1 - \sigma_3 = \frac{\varepsilon_a}{a + b\varepsilon_a} = \frac{1}{(a/\varepsilon_a) + b} \quad (11)$$

where: $\sigma_1 - \sigma_3$ represents the axial deviatoric stress, ε_a represents the axial strain and a and b are material coefficients.

$\varepsilon_a \otimes \forall$ asymptote of the stress-strain curves can be obtained; namely, the ultimate deviating stress $(\sigma_1 - \sigma_3)_{ult}$, which shows that the relationship between the ultimate deviatoric stress and the maximum deviatoric stress is generally in direct proportion. As depicted in Fig. 7(a), the ultimate deviatoric stress $(\sigma_1 - \sigma_3)_{ult}$ and confining pressure σ_3 can be described by the following equation:

$$(\sigma_1 - \sigma_3)_{ult} = \frac{1}{b} = \sigma_{ult} + ue^{-(\sigma_3/m)} \quad (12)$$

where: $(\sigma_1 - \sigma_3)_{ult}$ is the ultimate deviatoric stress, σ_{ult} , u and t are fitting coefficients and b is the inverse of the ultimate deviatoric stress $(\sigma_1 - \sigma_3)_{ult}$. In this study, $\sigma_{ult} = 11.90$, $u = 144.04$, $m = 1.50$, $R^2 = 0.996$.

Because σ_3 is constant in Eq. (11), the tangent modulus E_t can be expressed as:

$$E_t = \frac{d(\sigma_1 - \sigma_3)}{d\varepsilon_a} = \frac{a}{(a + b\varepsilon_a)^2} \quad (13)$$

When the axial strain $\varepsilon_a \rightarrow 0$, initial deformation modulus E_i of the stress-strain curves can be computed as follows:

$$E_i = \left[\frac{a}{(a + b\varepsilon_a)^2} \right]_{\varepsilon_a \rightarrow 0} = \frac{1}{a} \quad (14)$$

From Eq. (14), it can be deduced that a represents the reciprocal of the initial deformation modulus E_i .

The relationship between the initial deformation modulus E_i and confining pressure σ_3 is depicted in Fig. 7(b). According to relevant research (Janbu, 1963; Stamatopoulos and Kotzias, 1978), it can be

characterized by the following formula:

$$E_i = K_E p_a \left(\frac{\sigma_3}{p_a} \right)^k \quad (15)$$

or:

$$\lg \frac{E_i}{p_a} = \lg K_E + k \lg \frac{\sigma_3}{p_a} \quad (16)$$

where: K_E and k are material parameters, p_a represents the standard atmospheric pressure, $p_a = 0.10133 \text{ MPa}$, while $\lg K_E$ and k represent the intercept and slope of the fitted curve, respectively. In this study, $\lg K_E = 4.113$, $k = 0.448$, $R^2 = 0.966$.

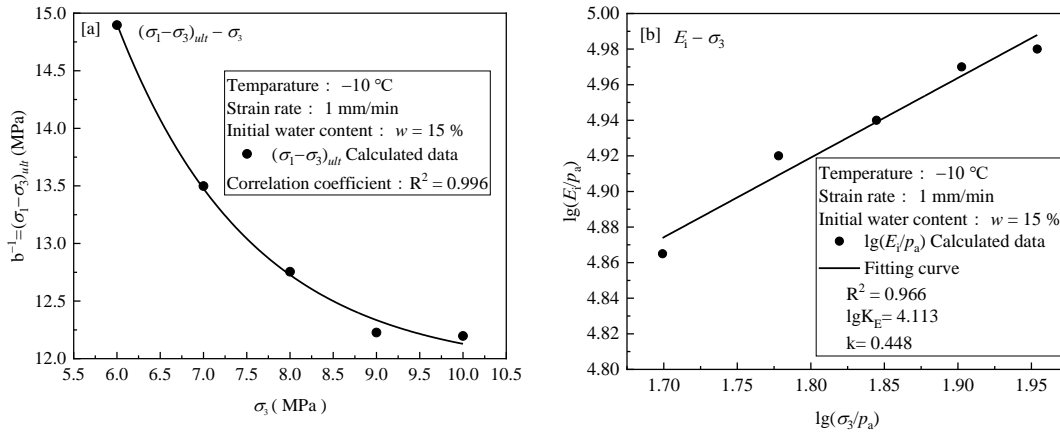


Figure (7): The relationship between ultimate deviatoric stress $(\sigma_1 - \sigma_3)_{ult}$, initial deformation modulus E_i and confining pressure σ_3

The failure deviatoric stress ratio R_f was introduced to determine the ultimate deviatoric stress $(\sigma_1 - \sigma_3)_{ult}$ (Sun et al., 2014):

$$R_f = \frac{(\sigma_1 - \sigma_3)_f}{(\sigma_1 - \sigma_3)_{ult}} \quad (17)$$

or:

$$(\sigma_1 - \sigma_3)_f = (\sigma_1 - \sigma_3)_{max} = \sigma_0 + m e^{-(\sigma_3/n)} \quad (18)$$

Normally, $R_f = 0.75 \sim 1.0$.

The tangent modulus E_t can be calculated by substituting Eqs. (15) ~ (18) into Eq. (13):

$$E_t = K_E p_a \left(\frac{\sigma_3}{p_a} \right)^k \left[1 - \frac{R_f (\sigma_1 - \sigma_3)}{\sigma_0 + m e^{-(\sigma_3/n)}} \right]^2 \quad (19)$$

To verify the validity of the model, the calculated data obtained using the Duncan-Chang model and the experimental data are shown in Fig. 8(a-e) and Table 2. Through comparative analysis, it was found that the calculated data and the experimental data are in good agreement, which enables a better reflection of the strength-deformation characteristics of frozen saline soil under high confining-pressure conditions and can provide a reference for engineering construction in this region.

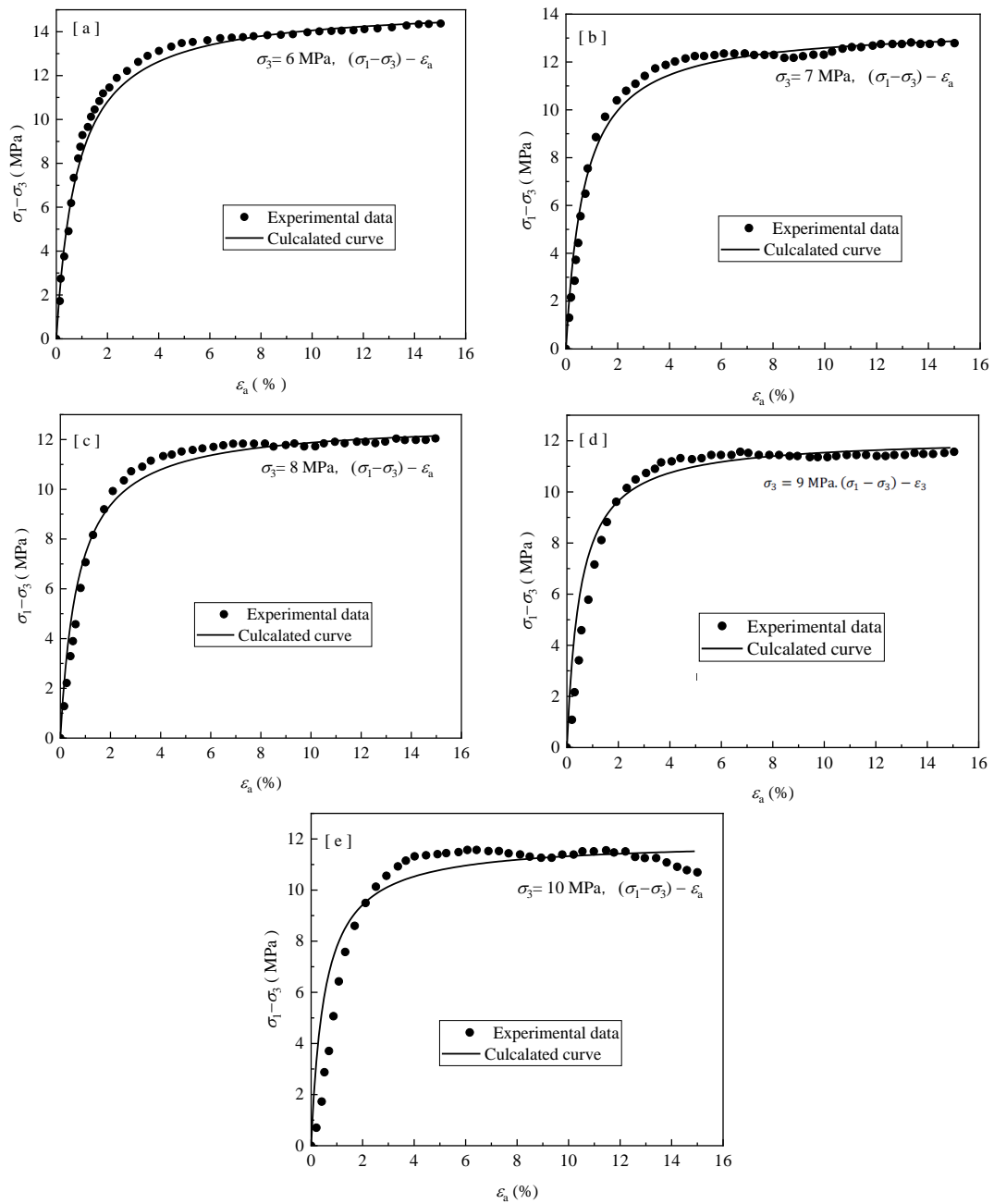


Figure (8): Comparison of experimental results and calculated results

Table 2. Comparison of calculation results with typical test results

ε_a	$\sigma_1 - \sigma_3$	$\sigma_3 = 6 \text{ MPa}$		$\sigma_1 - \sigma_3$	$\sigma_3 = 7 \text{ MPa}$	
/%	Test value	Calculated value	Deviation /%	Test value	Calculated value	Deviation /%
0.5	6.190	5.794	6.84	5.148	5.597	-8.02
1.0	9.280	8.387	5.01	8.432	7.909	6.61
2.0	11.450	10.810	5.90	10.496	9.967	5.31
4.0	13.125	12.635	3.89	11.964	11.459	4.41
8.0	13.840	13.800	0.29	12.298	12.385	-0.70
12.0	14.112	14.238	-2.88	12.749	12.728	0.17

CONCLUSIONS

The widely distributed sulfate saline soil in the Hexi region of Gansu province was used as the research object and the effect of high confining pressure on the shear strength-deformation characteristics of frozen saline silty clay was studied. The conclusions drawn are as follows:

- 1) The stress-strain curves of the frozen sulfate saline silty clay were hyperbolic and the failure mode was plastic failure. The deviatoric stress increased gradually as the axial strain increased and finally remained constant. When the confining pressure $\sigma_3 > 6$ MPa, the strength of frozen soil decreased with increased confining pressure. The reason was that on the one hand, ice melting and the resulting pore-water pressure reduced the ice bonding force and internal friction force between soil particles and on the other hand, the excess pore-water pressure generated by ice melting reduced the normal stress on the shear plane. The presence of salt decreases the strength of soil and the higher the salt content, the more the strength decreased.
- 2) The sample exhibits volume shrinkage over the entire confining-pressure range. As the axial strain increased, the volumetric strain rapidly increased and then slowly increased until the sample underwent shear failure. Before applying shear stress to the sample, it has completed consolidation and the greater the confining pressure, the denser the sample. Similarly, the greater the confining pressure, the greater the ability to limit shear deformation when shear stress is applied.
- 3) The failure strength of frozen sulfate saline silty clay under high confining pressure was determined. A strength criterion for frozen sulfate saline silty clay was proposed based on the test results. From the relationship between Mohr's circle and the shear strength curve, it is found that this criterion can accurately reflect the failure strength of saline frozen silty clay under various confining pressures.
- 4) The Duncan-Chang model was used to illustrate the strength-deformation characteristics of frozen sulfate saline silty clay under a high confining pressure. A comparison between the test data and the model prediction results confirms that the model can well depict the strength-deformation behavior of saline silty clay in the Hexi region of Gansu province, China.

Conflict of Interests

The authors declare that there is no conflict of interests regarding the publication of this paper.

Data-availability Statement

The experimental data in this paper are obtained from my own experimental results.

Acknowledgements

This research was supported by the National Natural Science Foundation of China (11962016 and 51978320) and by the Foundation for Innovation Groups of Basic Research in Gansu Province (20JR5RA478). The authors are grateful to the reviewers as well as to the editor for their insightful and constructive comments.

REFERENCES

- Cai, Z.Y., Wu, Z.Q., Huang, Y.H., Cao, Y.Y., and Wei, Y.B. (2014). "Influence of water and salt contents on strength of frozen soils." [In Chinese]. *Chinese Journal of Geotechnical Engineering*, 36 (9), 1580-1586.
- Chang, D., Lai, Y.M., and Zhang, M.Y. (2019). "A meso-macroscopic constitutive model of frozen saline sandy soil based on homogenization theory." *International Journal of Mechanical Sciences*, 159, 246-259. <https://doi.org/10.1016/j.ijmecsci.2019.06.002>.
- Fu, G.H., Deng, Z.W., and Tang, J. (2020). "Analysis of lacustrine facies soft soil roadbed settlement based on a viscoelastic-plastic model". *Jordan Journal of Civil Engineering*, 14 (1), 57-68.
- Gao, J., Lai, Y.M., Chang, D., and Niu, Y.Q. (2019). "Strength criterion for frozen saline sand considering effects of loading rates." [In Chinese]. *Chinese Journal of Geotechnical Engineering*, 41 (1), 104-110.
- Gao, J., and Lai, Y.M. (2018). "Damage and pressure-melting analysis of frozen saline soils in the process of triaxial-compression tests." [In Chinese]. *Chinese Journal of Geotechnical Engineering*, 40 (4), 707-715.

- Han, Y., Wang, Q., Wang, Ning., Wang, J.Q., Zhang, X.D., Cheng, S.K., and Kong, Y.Y. (2018). "Effect of freeze-thaw cycles on shear strength of saline soil." *Cold Regions Science and Technology*, 154, 42-53. <https://doi.org/10.1016/j.coldregions.2018.06.002>
- He, J.L., Niu, F.J., Luo, F., and Jiang, H.Q. (2022). "Effects of temperature and confining pressure on mechanical characteristics of frozen gravelly soil." *Jordan Journal of Civil Engineering*, 16 (2), 242-253.
- Hu, K., and Lai, Y.M. (2014). "Experimental study on the strength parameters and strength criterion of saline frozen silty sand." [In Chinese]. *Journal of Glaciology and Geocryology*, 36 (5), 1199-1204.
- Janbu, N. (1963). "Soil compressibility as determined by oedometer and triaxial tests." *Proceedings of the ECSMFE, Wiesbaden*, 83-87.
- Lai, Y.M., Cheng, H.B., Gao, Z.H., Zhang, S.J., and Chang, X.X. (2007). "Stress-strain relationships and nonlinear Mohr strength criterion of frozen sand clay." [In Chinese]. *Chinese Journal of Rock Mechanics and Engineering*, 26 (8), 1612-1617.
- Lai, Y.M., Jin, L., and Chang, X.X. (2009). "Yield criterion and elastoplastic-damage constitutive model for frozen sandy soil." *International Journal of Plasticity*, 25 (6), 1177-1205.
- Liao, M.K., Lai, Y.M., and Wang, C. (2016). "A strength criterion for frozen sodium sulfate saline soil." *Canadian Geotechnical Journal*, 53 (7), 1176-1185. <https://doi.org/10.1139/cgj-2015-0569>.
- Liu, X.Y., Liu, E.L., Zhang, D., Zhang, G., and Song, B.T. (2019). "Study on strength criterion for frozen soil." *Cold Regions Science and Technology*, 161, 1-20. <https://doi.org/10.1016/j.coldregions.2019.02.009>.
- Luo, F., Liu, E.L., and Zhu, Z.Y. (2019). "A strength criterion for frozen moraine soils." *Cold Regions Science Technology*, 164, 1-11. <https://doi.org/10.1016/j.coldregions.2019.102786>.
- Ma, W., and Chang, X.X. (2002). "Analyses of strength and deformation of an artificially-frozen soil wall in underground engineering." *Cold Regions Science Technology*, 34 (1), 11-17.
- Niu, Y.Q., Wang, X., Liao, M.K., and Chang, D. (2022). "Strength criterion for frozen silty clay considering the effect of initial water content." *Cold Regions Science Technology*, 34 (1), 1-9. <https://doi.org/10.1016/j.coldregions.2022.103521>
- Stamatopoulos, A.C., and Kotzias, P.C. (1978). "Soil compressibility as measured in the oedometer." *Géotechnique*, 28 (4), 363-375.
- Sun, G.Y., Yang, P., and Liu, R.G. (2014). "Experimental test on constitutive relationship of Nanjing frozen silty clay considering Duncan -Chang model." [In Chinese]. *Chinese Journal of Rock Mechanics and Engineering*, 33 (S1), 2889-2995.
- Xu, J., Li, Y.F., Lan, W., and Wang, S.H. (2019). "Shear strength and damage mechanism of saline intact loess after freeze-thaw cycling". *Cold Regions Science and Technology*, 164, 1-13. <https://doi.org/10.1016/j.coldregions.2019.05.005>.
- Xu, J., Liu, H., and Zhao, X.K. (2017). "Study on the strength and deformation property of frozen silty sand with NaCl under triaxial-compression condition". *Cold Regions Science and Technology*, 137, 7-16. <http://dx.doi.org/10.1016/j.coldregions.2017.01.008>.
- Xu, X.T., Li, Q.L., Lai, Y., Pang, W.T., and Zhang, R.P. (2019). "Effect of moisture content on mechanical and damage behavior of frozen loess under triaxial condition along with different confining pressures." *Cold Regions Science and Technology*, 157, 110-118. <https://doi.org/10.1016/j.coldregions.2018.10.004>.
- Xu, X.T., Wang, Y.B., Bai, R.Q., Fan, C.X., and Huang, S.G. (2016). "Comparative studies on mechanical behavior of frozen natural saline silty sand and frozen desalted silty sand". *Cold Regions Science and Technology*, 132: 81-88. <http://dx.doi.org/10.1016/j.coldregions.2016.09.015>.
- Yang, C.S., He, P., Cheng, G.D., Zhao, S.P., and Deng, Y.S. (2008). "Study of stress-strain relationships and strength characteristics of saturated saline frozen silty clay". [In Chinese]. *Rock and Soil Mechanics*, 29 (12), 3282-3286.
- Yang, J.S. (2008). "Development and prospect of research on salt-affected soils in China." [In Chinese]. *Acta Pedologica Sinica*, 45 (5), 837-845.
- Zhang, D., Liu, E.L., Liu, X.Y., Zhang, G., and Song, B.T. (2017). "A new strength criterion for frozen soils considering the influence of temperature and coarse-grained contents". *Cold Regions Science and Technology*, 143, 1-12. <http://dx.doi.org/10.1016/j.coldregions.2017.08.006>.

- Zhang, W.B., Ma, J.Z., and Tang, L. (2019). "Experimental study on shear strength characteristics of sulfate saline soil in Ningxia region under long-term freeze-thaw cycles". *Cold Regions Science and Technology*, 160, 48-57. <https://doi.org/10.1016/j.coldregions>. 2019. 01.008.
- Zhang, Y.Q., Yang, P., Jiang, W.Y., and Zhang, T. (2019). "Study on triaxial strength and constitutive model of frozen silty clay". [In Chinese]. *China Civil Engineering Journal*, 52 (S1), 8-15.
- Zhao, Y.H., Lai, Y.M., Pei, W.S., and Yu, F. (2020a). "An anisotropic bounding surface elastoplastic constitutive model for frozen sulfate saline silty clay under cyclic loading". *International Journal of Plasticity*, 129 (4), 1-32. <https://doi.org/10.1016/j.ijplas>. 2020. 102668.
- Zhao, Y.H., Lai, Y.M., Zhang, J., and Liao, M.K. (2020b). "A dynamic strength criterion for frozen sulfate saline silty clay under cyclic loading". *Cold Regions Science and Technology*, 173, 1-13. <https://doi.org/10.1016/j.coldregions>. 2020. 103026.